

Charging and Spin Effects in Triple Dot Artificial Molecules

A. Vidan,¹ R. M. Westervelt,¹ M. Stopa,² M. Hanson,³ and A. C. Gossard³

Received 20 August 2004; accepted 29 September 2004

We have fabricated artificial molecules consisting of three coupled quantum dots defined in the two-dimensional electron gas of a GaAs/AlGaAs heterostructure using lithographically patterned gates and trenches. The three dots are arranged in a ring structure, where each dot is coupled to the other two dots. We find that, when tuned to the Coulomb blockade regime, the triple quantum dot device acts as a charge rectifier: an electron enters the third dot where it is trapped, producing a jamming effect where no other electron may enter the first dot. Triple quantum dots coupled in a ring will allow for the study of new molecular phases using artificial molecules and may also serve as building blocks of two-dimensional arrays for quantum computation.

KEY WORDS: quantum dot; Coulomb blockade; single-electron tunneling; rectification.

1. INTRODUCTION

Semiconductor quantum dots are commonly referred to as artificial atoms: nanostructured devices where electrons are spatially confined and occupy discrete energy levels [1]. These artificial atoms are tunable, in that their shape, size, and electron density can be modified [2]. When two or more artificial atoms are allowed to interact, either by allowing electrons to tunnel between them or by a capacitive effect, artificial molecules are formed. For example, a system of two coupled quantum dots can be used to study how a molecular bond is formed as a function of electron tunneling between the individual artificial atoms, and an analog of the molecular binding energy can be measured [3].

Quantum dots may also be used as building blocks for nanometer scale electronic circuits [4]. One advantage of using semiconductor quantum dots is scalability: making quantum dots smaller only enhances their properties and reduces their, already

low, power consumption. Furthermore, spins of localized electrons in quantum dots can serve as qubits for quantum information storage and processing [5]. Quantum computation, and the ability to have error correction, will require *many* qubits coupled together. In the last decade, coupled quantum dots in a *linear* arrangement have been studied thoroughly [6]. However, the need for many qubits will require having *two-dimensional* arrays of coupled dots. One such arrangement may be a triangular lattice of dots, as shown in Fig. 1. In this paper, we consider a unit cell of such an array. This unit cell consists of three quantum dots placed at the corners of an equilateral triangle.

2. TRIPLE QUANTUM DOT DEVICES

Figure 1 shows scanning electron micrographs of two different implementations of the triple quantum dot (TQD) unit cell. For both devices, lithographically patterned Cr:Au gates are used to define three quantum dots in a GaAs/Al_{0.3}Ga_{0.7}As heterostructure containing a two-dimensional electron gas (2DEG). For the device shown in Fig. 1(b) (TQD1), an ion-etched trench, 30 nm deep, is used to deplete the 2DEG, located 52 nm below the surface, in the center region. At 4 K, the 2DEG sheet carrier

¹Division of Engineering and Applied Sciences and Department of Physics, Harvard University, Cambridge, Massachusetts 02138; e-mail: westervelt@deas.harvard.edu.

²Tarucha Mesoscopic Correlation Project, ERATO-JST, NTT Atsugi Research and Development Laboratories, Japan.

³Materials Department, University of California at Santa Barbara, California 93106.

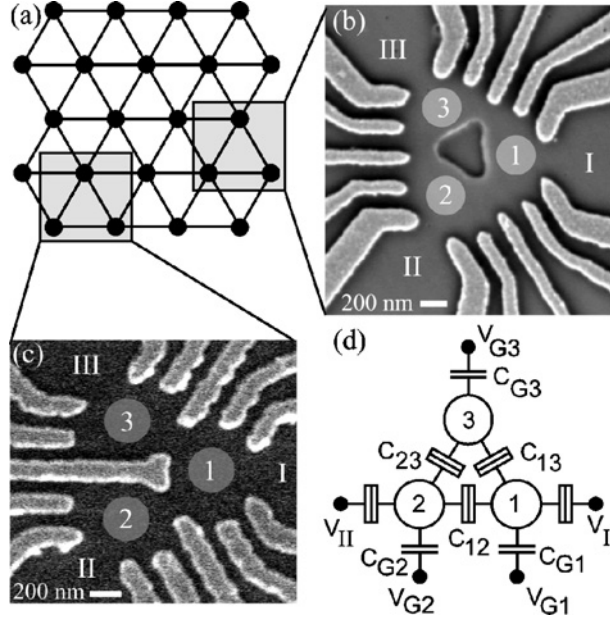


Fig. 1. (a) Triangular lattice for a two-dimensional array of coupled dots. Highlighted regions are two triple quantum dot unit cells. SEM images of triple quantum dot (b) device 1 (TQD1) and (c) device 2 (TQD2) are shown. Light grey areas are tunable metal gates. Dark center region in (b) is a 30 nm ion-etched trench. Dot locations are marked by the circles. (d) Circuit model of a triple quantum dot. Split boxes represent tunnel junctions. Each quantum dot ($i = 1, 2, 3$), with total capacitance C_i , is capacitively-coupled to a side gate, with gate voltage V_{Gi} and capacitance C_{Gi} . Cross-capacitances are neglected. For TQD2, C_{23} is a pure capacitor.

density and mobility are $n_s = 3.8 \times 10^{11} \text{ cm}^{-2}$ and $\mu = 460000 \text{ cm}^2 \text{ V}^{-1} \text{ s}^{-1}$. For the device shown in Fig. 1(c) (TQD2), the 2DEG is located 57 nm below the surface, with a low-temperature sheet carrier density and mobility of $n_s = 4.5 \times 10^{11} \text{ cm}^{-2}$ and $\mu = 400000 \text{ cm}^2 \text{ V}^{-1} \text{ s}^{-1}$.

The main difference between the two triple dot devices shown in Fig. 1 is that TQD1 allows for tunnel-coupling between any two dots. TQD2 allows for tunneling only between dots 1 and 2 and dots 1 and 3. No exchange of electrons is allowed between dots 2 and 3 because of the infinite barrier resulting from the center metal gate. However, dots 2 and 3 interact capacitively [7].

It is useful to consider the stability, or charging, diagram of a triple quantum dot, as is normally done for double quantum dots [6, 8]. To obtain the stability diagram, in the (classical) linear regime, we begin with the electrostatic energy of the system, assuming negligible cross-capacitances and zero source-drain

voltage:

$$U(N_1, N_2, N_3) = \sum_{i=1}^3 \frac{1}{2} E_i N_i^2 + \sum_{i<j=2}^3 N_i N_j E_{ij} + f(V_{G1}, V_{G2}, V_{G3}) \quad (1)$$

where N_i is the number of electrons in dot i . The first term represents the charging energy of the three individual dots, with

$$E_i = \frac{e^2}{C_i} \left(1 - \frac{2C_{12}C_{13}C_{23} + C_j C_{ik}^2 + C_k C_{ij}^2}{C_1 C_2 C_3 - C_i C_{jk}^2} \right)^{-1} \quad (2)$$

Note that this is the usual charging energy for the uncoupled dot i , multiplied by a factor due to the coupling caused by dots j and k . The second term in Eq. (1) represents the electrostatic coupling energy between dot i and dot j , in the presence of dot k , for the three pairs, given by

$$E_{ij} = \frac{e^2 (C_{ij} C_k + C_{ik} C_{jk})}{C_1 C_2 C_3 - 2C_{12} C_{13} C_{23} - C_1 C_{23}^2 - C_2 C_{13}^2 - C_3 C_{12}^2} \quad (3)$$

$f(V_{G1}, V_{G2}, V_{G3})$ is the electrostatic energy due to the induced charge caused by the gate voltages:

$$\begin{aligned} f(V_{G1}, V_{G2}, V_{G3}) = & \frac{1}{2e^2} (C_{G1}^2 V_{G1}^2 E_{c1} + C_{G2}^2 V_{G2}^2 E_{c2} \\ & + C_{G3}^2 V_{G3}^2 E_{c3}) + \frac{1}{e^2} (C_{G1} V_{G1} C_{G2} V_{G2} E_{c12} \\ & + C_{G1} V_{G1} C_{G3} V_{G3} E_{c13} + C_{G2} V_{G2} C_{G3} V_{G3} E_{c23}) \\ & - \frac{1}{e} C_{G1} V_{G1} (N_1 E_{c1} + N_2 E_{c12} + N_3 E_{c13}) \\ & - \frac{1}{e} C_{G2} V_{G2} (N_1 E_{c12} + N_2 E_{c2} + N_3 E_{c23}) \\ & - \frac{1}{e} C_{G3} V_{G3} (N_1 E_{c13} + N_2 E_{c23} + N_3 E_{c3}) \end{aligned} \quad (4)$$

All other terms are defined in Fig. 1(d). The electrochemical potential for each dot equals the energy needed to add the N_i th electron on dot i while having N_j and N_k electrons on dot j and dot k . For example, for dot 1, we have

$$\begin{aligned} \mu(N_1, N_2, N_3) \equiv & U(N_1, N_2, N_3) - U(N_1 - 1, N_2, N_3) \\ = & \left(N_1 - \frac{1}{2} \right) E_{c1} + N_2 E_{c12} + N_3 E_{c13} \\ & - \frac{1}{e} (C_{G1} V_{G1} E_{c1} + C_{G2} V_{G2} E_{c12} + C_{G3} V_{G3} E_{c13}) \end{aligned} \quad (5)$$

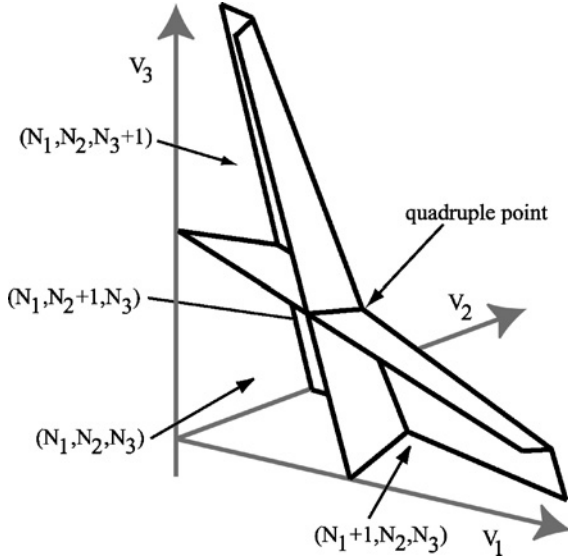


Fig. 2. First cell of the stability (charging) diagram of a triple quantum dot, showing the charge configuration versus the three independent side gate voltages.

For negligible source-drain voltage across the triple dot, the electrochemical potential of the leads can be set to zero. Stable states of the triple quantum dot occur when the N_i 's take on the largest possible *integer* values while maintaining a negative electrochemical potential for each dot. The stability diagram is shown in Fig. 2. There exists a 'quadruple point' where the four states (N_1, N_2, N_3) , $(N_1 + 1, N_2, N_3)$, $(N_1, N_2 + 1, N_3)$, and $(N_1, N_2, N_3 + 1)$ are degenerate. This is similar to a double dot system, which exhibits a triple point. Measuring the stability diagram of triple dots, coupled as a ring, will allow for the study of the electronic states of this new type of artificial molecule.

Certain lattice geometries frustrate the spin-spin interactions. For nearest neighbor antiferromagnetic coupling of spins in the triple dot molecule, the system is unable to satisfy all pairwise interactions. The ground state energy of the triple dot molecule is the same for six different spin configurations, where two of the three spins must point in the same direction. This situation is known as geometric spin frustration [9]. Typically, it is difficult to study geometric spin frustration because defects and three-dimensional inter-coupling normally act to relieve the frustration in real materials. An artificially engineered two-dimensional structure will provide a model system in which to study geometric spin frustration.

We propose to study geometric spin frustration in the triple quantum dot of Fig. 1(b), with exchange interactions described by an effective spin Hamiltonian $H = -(J_{12}\mathbf{S}_1 \cdot \mathbf{S}_2 + J_{13}\mathbf{S}_1 \cdot \mathbf{S}_3 + J_{23}\mathbf{S}_2 \cdot \mathbf{S}_3)$. \mathbf{S}_i is the spin on dot i and J_{12} , J_{13} , and J_{23} are negative. The Cr:Au gates of the three inter-dot quantum point contacts are fully tunable, and allow control over each individual exchange coupling J_{ij} [10]. Therefore, we can perform transport measurements of a frustrated triple dot ($J_{12} = J_{13} = J_{23}$) and then relieve the frustration by tuning one exchange coupling to zero. Aside from conventional conductance measurements, including spin blockade spectroscopy using spin polarized leads [11], we believe measurements of the thermopower of the triple dot molecule may reveal spin frustration characteristics [12]. The thermopower S is the ratio of the voltage build-up V to the thermal gradient T under the condition of zero current. Thermopower of quantum dots in the Coulomb blockade regime has been studied theoretically [13] and has been used as an effective spectroscopic tool [14]. Thermopower of a quantum dot embedded in a ring has also been considered [15].

3. SINGLE-ELECTRON TUNNELING AND RATCHET EFFECTS

We operate the triple quantum dot devices in the Coulomb blockade regime. All measurements were done in a Helium-3 system at the base temperature of 380 mK. Figure 3 shows the addition spectrum for TQD1, measured through leads I and II while completely isolating dot 3 from lead III. All three inter-dot quantum point contacts are set to $\sim 2 e^2/h$, thereby having the triple dot act as one big dot, with the usual finite-bias Coulomb blockade diamonds observed. From the data, we find that the total self-capacitance of the single large composite dot is ~ 615 aF, corresponding to a charging energy of 0.26 meV. From separate measurements, we find the total capacitance for a single dot to be ~ 256 aF, corresponding to a charging energy of 0.625 meV. From finite-bias Coulomb blockade measurements of a single dot of TQD2 we find a total dot capacitance of 310 aF, corresponding to a charging energy of 0.515 meV. We note that due to lateral depletion of the ion-etched trench, the actual dot sizes in TQD1 are smaller than the lithographic sizes expected, resulting in smaller dots and larger charging energies.

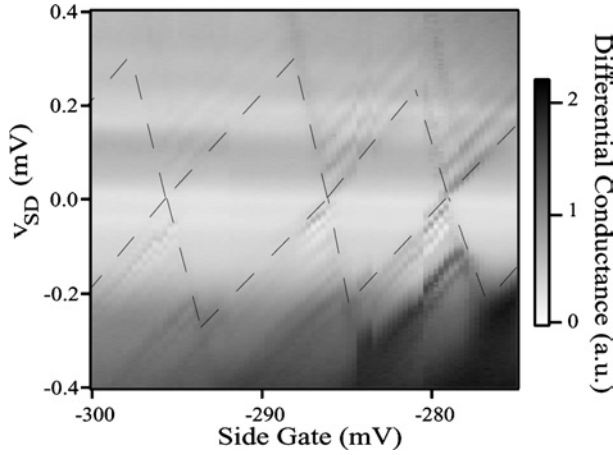


Fig. 3. Differential conductance of TQD1 acting as one large composite dot. All inter-dot quantum point contacts are set to $\sim 2 e^2/h$. Dot 3 is completely isolated from lead III. Differential conductance is measured as a function of all six side gates and the dc bias, $V_{SD} = V_{II} - V_I$. The diamonds, highlighted by dashed lines for clarity, are Coulomb blocked regions where current through the triple dot is zero. Lines parallel to the diamonds are excited states of the triple quantum dot.

The asymmetric configuration of TQD2 allows it to function as a *Coulomb blockade charging ratchet*, as proposed in Ref. [16]. The main feature of a ratchet is a breaking of symmetry under inversion [17]. Here, an asymmetry is present because no tunneling can take place between dots 2 and 3. Tunnel junction C_{23} in Fig. 1(d) is now a pure capacitor. With dot 3 isolated from its lead, it effectively acts as a quantum box, tunnel-coupled with dot 1. By measuring the current through the triple dot device, as a function of the applied voltage across dots 1 and 2, we find that the forward current is suppressed due to charging of this quantum box.

In order that TQD2 act as a charging ratchet, it is crucial to tune it to the quadruple point. This ensures that zero or only one *excess* electron is allowed inside the triple quantum dot at any given time. Once tuned to the quadruple point, a current can flow only as electrons pass through the triple dot *one at a time*, as shown in Fig. 4. For forward bias, an electron that enters dot 3, gets trapped and suppresses current flow. For reverse bias, no trapping occurs. We have recently been able to demonstrate this rectification effect experimentally [18]. A Monte-Carlo simulation of the I-V characteristics of our device, employing capacitances derived from the self-consistent simulation of the full 3D structure, including wafer profile and the device surface gate pattern, is shown

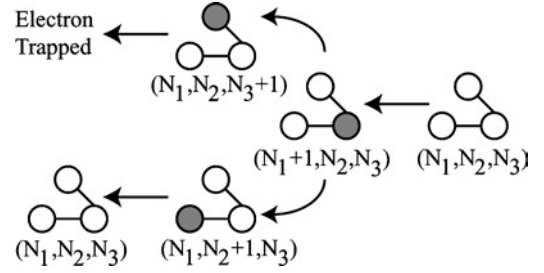


Fig. 4. Schematic diagram showing jamming process for the triple quantum dot charging ratchet. At the quadruple point, only these four degenerate states are accessible. A small forward bias breaks this degeneracy, and allows for an electron to be trapped in dot 3. Current can flow only if the electron follows the lower path. For reverse bias no trapping occurs.

in Fig. 5 [16,19]. The measured I-V characteristics agree well with simulations. We find that the current is symmetric around zero bias, due to the degeneracy of the quadruple point. For negative bias, current is not suppressed. For positive bias, after a region of negative differential resistance, the current is suppressed due to the jamming effect. For large positive bias, the triple dot is pushed away from the quadruple point, and many electrons are allowed in the device.

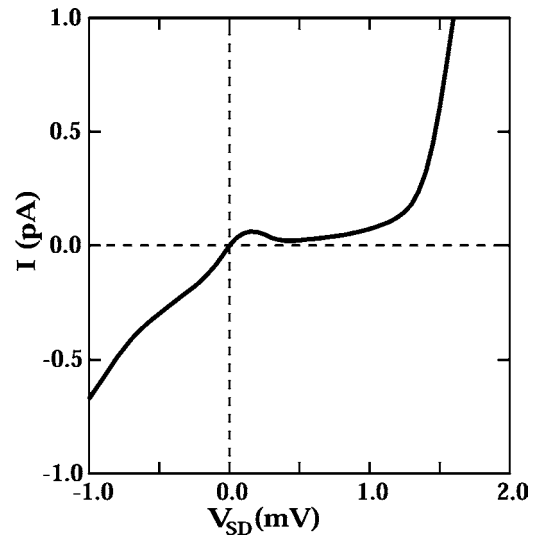


Fig. 5. Monte Carlo simulation of the triple quantum dot I-V characteristics at $T = 450$ mK. Dot 3 is isolated from lead III, and a current is measured versus applied voltage $V_{SD} = V_{II} - V_I$. Current suppression and negative differential resistance for $V_{SD} > 0$ is found. Parameters used in the simulation are calculated from a self-consistent simulation of the full 3D structure of our device: $C_1 = C_2 = 200$ aF, $C_3 = 105$ aF, $C_{23} = 50$ aF.

4. SUMMARY

Triple quantum dots are new types of artificial molecules, compared to the previously studied one-dimensional coupled-dots in series. Recently, it has been proposed to use a triple quantum dot to create spin-entangled currents [20]. We have presented two different configurations of a triple quantum dot system, which may be used as building blocks of a two dimensional array for solid state quantum computation. Furthermore, the asymmetric configuration introduced in the triple quantum dot results in a bias-dependent current suppression, making this a promising candidate as a single-electron rectifier in future single-electron tunneling device circuits.

ACKNOWLEDGMENTS

This work was supported by the DARPA QuIST program (DAAD19-01-1-0659) at Harvard, iQUEST at UC Santa Barbara, and the Nanoscale Science and Engineering Center (NSF PHY-01-17795) based at Harvard.

REFERENCES

1. M. A. Kastner, *Physics Today* **46**, 24 (1993).
2. L. P. Kouwenhoven, C. M. Marcus, P. McEuen, S. Tarucha, R. M. Westervelt, and N. Wingreen, in *Mesoscopic Electron*

- Transport*, L. L. Sohn, L. P. Kouwenhoven, and G. Schön, eds. (Kluwer, 1997), p. 105.
3. C. Livermore, C. H. Crouch, R. M. Westervelt, K. L. Campman, and A. C. Gossard, *Science* **274**, 1332 (1996).
 4. K. K. Likharev, *Proceedings of the IEEE* **87**, 606 (1999).
 5. D. Loss and D. P. DiVincenzo, *Phys. Rev. A* **57**, 120 (1998).
 6. W. G. van der Wiel, S. De Franceschi, J. M. Elzerman, T. Fujisawa, S. Tarucha, and L. P. Kouwenhoven, *Rev. Mod. Phys.* **75**, 1 (2003), and references therein.
 7. I. H. Chan, R. M. Westervelt, K. D. Maranowski, and A. C. Gossard, *Appl. Phys. Lett.* **80**, 1818 (2002).
 8. H. Pothier, P. Lafarge, C. Urbina, D. Esteve, and M. H. Devoret, *Europhys. Lett.* **17**, 249 (1992); I. M. Ruzin, V. Chandrasekhar, E. I. Levin, and L. I. Glazman, *Phys. Rev. B* **45**, 13469 (1992).
 9. A. Harrison, *J. Phys.: Condens. Matter* **16**, S553 (2004), and the references cited therein.
 10. G. Burkard, D. Loss, and D. P. DiVincenzo, *Phys. Rev. B* **59**, 2070 (1999).
 11. M. Ciorga, A. S. Sachrajda, P. Hawrylak, C. Gould, P. Zawadzki, Y. Feng, and Z. Wasilewski, *Phys. Rev. B* **61**, R16315 (2000).
 12. Y. Wang, N. S. Rogado, R. J. Cava, and N. P. Ong, *Nature* **423**, 425 (2003).
 13. C. W. J. Beenakker and A. A. M. Staring, *Phys. Rev. B* **46**, 9667 (1992).
 14. A. S. Dzurak, C. G. Smith, C. H. W. Barnes, M. Pepper, L. Martin-Moreno, C. T. Liang, D. A. Ritchie, and G. A. C. Jones, *Phys. Rev. B* **55**, R10197 (1997).
 15. Ya. M. Blanter, C. Bruder, R. Fazio, and H. Schoeller, *Phys. Rev. B* **55**, 4069 (1997); T. Kim and S. Hershfield, *Phys. Rev. Lett.* **88**, 136601 (2002).
 16. M. Stopa, *Phys. Rev. Lett.* **88**, 146802 (2002).
 17. For a review, see P. Reimann, *Phys. Rep.* **361**, 57 (2002).
 18. A. Vidan, R. M. Westervelt, M. Stopa, M. Hanson, and A. C. Gossard, *Appl. Phys. Lett.* **85**, 3602 (2004).
 19. M. Stopa, *Phys. Rev. B* **54**, 13767 (1996).
 20. D. S. Saraga and D. Loss, *Phys. Rev. Lett.* **90**, 166803 (2003).